Crack-induced resistivity changes in cracked CNTs reinforced composites

L. Rodríguez-Tembleque*[1], F. García-Sánchez[2], E. García-Macías[3], F.C. Buroni[1], A. Sáez[1]

[1] *Escuela Técnica Superior de Ingeniería, Universidad de Sevilla, Camino de los Descubrimientos s/n , Sevilla 41092, Spain.*

[2] *Escuela de Ingenierías Industriales, Universidad de Málaga, Doctor Ortiz Ramos s/n, Málaga 29071, Spain.*

[3] *Department of Civil and Environmental Engineering, University of Perugia, Via G Duranti 93, Perugia 06125, Italy.*

Abstract

This paper presents the application of a dual Boundary Element (BE) approach to analyze how the presence of cracks in carbon nanotubes (CNTs) reinforced polymer composites does influence their electrical conductivity. The presence of cracks in such composite materials may not only compromise their structural integrity, but may as well alter their capability to act as reliable piezo-resistive sensors in novel structural health monitoring applications. The electromechanical constitutive properties of the composite are determined by a mixed micromechanics approach that permits to characterize both the elastic properties and the strain-induced alterations in the overall electrical conductivity of the CNTs reinforced composite. The parameters of such micromechanics approach are adjusted to ensure a good fitting against experimental results available in the literature. The implemented dual BE formulation is based on both the displacement and traction boundary integral equations together with an efficient regularization procedure that permits to deal with the singular and hypersingular integrals in a straightforward manner. Discontinuous quarter-point elements are used to accurately evaluate the relevant fracture parameters. Electrical conductivity in the cracked composite follows from its computed strain state. Several parametric studies are conducted to illustrate the influence of various crack geometries in the piezo-resistive behavior of CNTs reinforced composites at varying CNTs concentrations.

Key words: Carbon Nanotube, Crack detection, Nanocomposites, piezoresistivity, Damage identification.

---

1. Introduction

Over the past fifteen years, composite materials fabricated by dispersing various carbon nano-scale fillers into a polymeric matrix, say for example graphene nanoplatelets or carbon nanotubes (CNTs), have attracted enormous attention from the scientific community. This is due to the fact that the electrical conductivity properties such fillers confer to the otherwise non-conductive matrix, make them good candidates as sensors for Structural Health Monitoring (SHM) applications. CNTs do not only reinforce the base matrix material by improving its overall mechanical properties, but also have the capability of forming –minimally invasive- electrically conductive networks that enable strain sensing [1, 2, 3, 4]. Recent advances on fabrication and testing ensure repeatability and stability of this new class of piezo-resistive sensors and establish them as an actual alternative for SHM [5, 6, 7].

For instance, previous works by the authors have satisfactorily illustrated the expected performance of multi-walled CNTs (MWCNT)/epoxy strip-like strain sensors for buckling detection in beam structures [8] and for crack detection and localization in reinforced concrete beams [9]. In this context, it is crucial to develop tools for assessing the structural integrity of the sensor itself, as cracks may appear within the MWCNT/epoxy strip sensor during its service life. In such a case, the problem that we face is twofold: the presence of a crack in the sensor will not only compromise its integrity, but it may significantly modify its sensing capability and therefore could lead to the adoption of wrong maintenance measures in a SHM framework.

*corresponding author
Email address: `luisroteso@us.es` (L. Rodríguez-Tembleque[1])

In this work, we aim at characterizing the change in electrical conductivity induced in a MWCNTs/epoxy composite by the presence of several crack configurations at varying CNTs volume fractions. For this purpose, the dual Boundary Element (BE) formulation previously developed by García-Sánchez et al. [10] for fracture mechanics applications in anisotropic materials is employed herein. The constitutive electro-mechanical modeling of the MWCNTs/epoxy composite follows a two-step procedure, whose details may be consulted elsewhere [8, 9]. In essence, provided that piezo-resistivity is a one-way coupled electro-mechanical property, we first conduct the homogenization of the mechanical properties by applying a mean-field approach that takes into account the interfacial effects that characterize the load transfer mechanisms at the epoxy matrix/MWCNT interfaces. The second step tackles the homogenization of the electrical conductivity and piezo-resistivity properties, implementing the model proposed by García-Macías et al. [11] and further adjusting the parameters of such micromechanics model to fit experimental results available in the literature [8, 9]. In this way, the dual BE approach computes the strain state in the cracked domain and subsequently strains are related to changes in piezo-resistivity. Several parametric studies are presented that reveal how the presence of cracks does significantly alter the piezo-resistive behavior of the MWCNTs/epoxy composite strain sensors.

2. Micromechanics modelling of MWCNT/epoxy nanocomposites

This section concisely overviews the micromechanics modelling of the electromechanical constitutive properties of strain self-sensing MWCNT/epoxy nanocomposites. For notational convenience, blackboard bold letters are used to denote fourth-order tensors $\mathbb{A} = A_{ijkl}$, while bold letters indicate second-order tensors $\mathbf{A} = A_{ij}$. A colon between two fourth-order tensors denotes inner product, $(\mathbb{A} : \mathbb{B})_{ijmn} \equiv A_{ijkl}B_{klmn}$.

2.1. *Mechanical properties of MWCNT/epoxy nanocomposites*

Let us assume a Representative Volume Element (RVE) of an epoxy matrix doped with a sufficient number of MWCNTs to statistically represent the composite as a whole. The geometrical dimensions of MWCNTs, that is length L_{cnt} and diameter D_{cnt}, are assumed constant throughout the RVE. The orientation of the fillers is unequivocally defined by two Euler angles, θ and γ as shown in Fig. 1 (a). In order to take into account the filler/matrix interfacial properties, a core-shell interphase model [12, 13] is adopted. This approach assumes that interfacial properties can be idealized as finite elastic coatings with constant thickness t surrounding the fillers. Therefore, the composite is defined as a three-phase composite including the matrix, inclusions and interphases with elastic tensors $\mathbb{C}_m$, $\mathbb{C}_p$ and $\mathbb{C}_i$. Indexes "p", "i", and "m" relate the corresponding quantity to the filler, interphase and matrix phases, respectively. According to the double inclusion methodology by Hori and Nemat-Nasser [14], the effective stiffness tensor of the composite reads:

$$\overline{\mathbb{C}} = \left(f_m\mathbb{C}_m + f_i \langle \mathbb{C}_i : \mathbb{A}_i\rangle + f_p \left\langle \mathbb{C}_p : \mathbb{A}_p\right\rangle\right) : \left(f_m\mathbb{I} + f_i \langle \mathbb{A}_i\rangle + f_p \left\langle \mathbb{A}_p\right\rangle\right)^{-1}, \tag{1}$$

with f_p, f_i, and f_m being the volume fractions occupied by the fillers, the interphases and the host matrix, respectively. MWCNT/epoxy interfaces are characterized by weak van der Waals (vdW) forces, thereby penetrable soft interphases are assumed in this work, and the expression of their volume fraction f_i can be found in references [15, 8]. Terms $\mathbb{A}_i$ and $\mathbb{A}_p$ in Eq. (1) denote the concentration tensors for interphases and inclusions, respectively, and can be expressed in terms of the corresponding dilute concentration tensors, $\mathbb{A}_i^{dil}$ and $\mathbb{A}_p^{dil}$, as:

$$\mathbb{A}_\chi = \mathbb{A}_\chi^{dil} : \left(f_m\mathbb{I} + f_i\mathbb{A}_i^{dil} + f_p\mathbb{A}_p^{dil}\right)^{-1}, \quad \chi = p, i \tag{2}$$

$$\mathbb{A}_\chi^{dil} = \mathbb{I} + \mathbb{S} : \mathbb{T}_\chi, \quad \chi = p, i \tag{3}$$

with

$$\mathbb{T}_\chi = -\left(\mathbb{S} + \mathbb{M}_\chi\right)^{-1}, \quad \chi = p, i \tag{4}$$

$$\mathbb{M}_\chi = \left(\mathbb{C}_\chi - \mathbb{C}_m\right)^{-1} : \mathbb{C}_m, \quad \chi = p, i \tag{5}$$

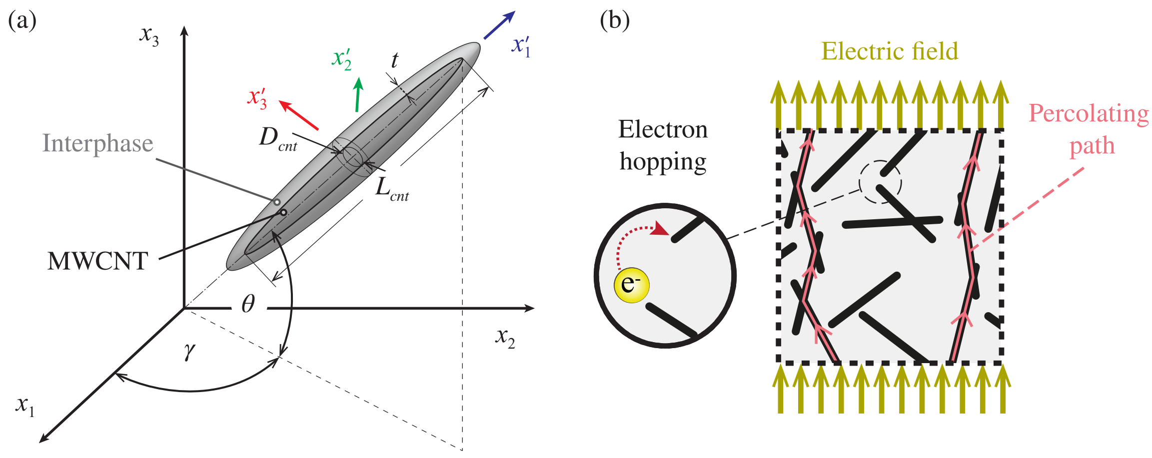

Figure 1: (a) Euler angles defining the relation between the orientation of a MWCNT in the local coordinate system, $K' \equiv \{0; x_1' x_2' x_3'\}$ and the global coordinate system, $K \equiv \{0; x_1 x_2 x_3\}$. (b) Schematic representation of the contribution of electron hopping and conductive networking mechanisms to the overall electrical conductivity of MWCNT/epoxy nanocomposites.

where $\mathbb{S}$ denotes the mechanical fourth-order Eshelby's tensor, whose formulation for prolate ellipsoidal particles can be found elsewhere [16]. Angle brackets $\langle\cdot\rangle$ in Eq. (1) indicate orientational average weighted by an Orientation Distribution Function $\Omega(\gamma, \theta)$. Unless special aligning techniques are undertaken, fillers are usually randomly oriented throughout the composite, and the ODF is constant within the whole Euler space.

2.2. *Electrical conductivity of MWCNT/epoxy nanocomposites*

Most literature works agree to define the electrical behaviour of MWCNT-based composites as percolation-type, according to which their electrical conductivity experiences a rapid increase of several orders of magnitude when the filler concentration reaches a certain percolation threshold f_c. Below percolation ($f_p < f_c$), fillers are very distant and electrons can only be transferred through a quantum tunnelling effect, also known as electron hopping mechanism. Once the filler volume fraction reaches the percolation threshold ($f_p \geq f_c$), some fillers begin forming electrically conductive paths and the overall conductivity is governed by both electron hopping and conductive networking mechanisms as sketched in Fig. 1 (b). The fraction of percolated MWCNTs, ξ, can be approximated as [17]:

$$\xi = \begin{cases} 0, & 0 \leq f_p < f_c \\ \dfrac{f_p^{1/3} - f_c^{1/3}}{1 - f_c^{1/3}}, & f_c \leq f_p \leq 1 \end{cases} \tag{6}$$

The electron hopping mechanism can be taken into account by conductive interphases, whilst the conductive networking mechanism can be simulated through variations of the filler aspect ratio [18]. The electrical resistivity of the interphases is commonly computed by the generalized Simmons' formula [19]:

$$R_{int}(d_a) = \frac{d_a \hbar^2}{a e^2 \left(2m\lambda^{1/2}\right)} \exp\left(\frac{4\pi d_a}{\hbar} (2m\lambda)^{1/2}\right), \tag{7}$$

where m and e are the mass and the electric charge of the electron, respectively, λ is the height of the tunnelling potential barrier, a is the contact area of the fillers, $\hbar$ stands for the reduced Planck's constant, and d_a is the average inter-particle distance. Being d_c the maximum filler separation for tunnelling penetration of electrons, d_a is usually approximated in a piecewise form [18] as d_c and $d_c \left(f_c/f_p\right)^{1/3}$ below and above percolation, respectively. The thickness of the conductive interphases t_c, their electrical conductivity σ_{int}, and the volume fraction f_{eff} of the effective fillers (MWCNTs plus interphases) can be computed as [20, 18]:

$$t_c = \frac{1}{2} d_a, \quad \sigma_{int} = \frac{d_a}{a R_{int}(d_a)}, \quad f_{eff} = \frac{\left(D_{cnt} + 2t_c\right)^2 \left(L_{cnt} + 2t_c\right)}{D_{cnt}^2 L_{cnt}} f_p. \tag{8}$$

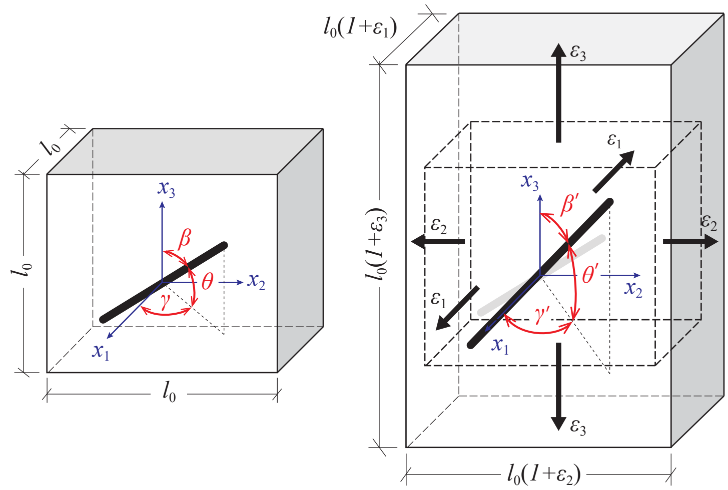

Figure 2: Cubic cell containing an embedded filler and deformed under a tri-axial strain state $(\varepsilon_1, \varepsilon_2, \varepsilon_3)$.

On this basis, MWCNT/interphase ensembles can be modelled through equivalent solid cylinders with transversely isotropic conductivity tensor $\boldsymbol{\sigma}_c$ (for more detailed information in this regard, readers may refer to [21, 18]). Hence, the overall electrical conductivity of the RVE can be estimated by the Mori-Tanaka method as [22, 23]:

$$\boldsymbol{\sigma}_{eff} = \boldsymbol{\sigma}_m + (1-\xi)\langle\boldsymbol{\Gamma}_{EH}\rangle + \xi\langle\boldsymbol{\Gamma}_{CN}\rangle, \tag{9}$$

where $\boldsymbol{\sigma}_m$ is the conductivity tensor of the matrix phase, and the matrices $\boldsymbol{\Gamma}_{EH}$ and $\boldsymbol{\Gamma}_{CN}$ read:

$$\boldsymbol{\Gamma}_{EH} = f_{eff}\,(\boldsymbol{\sigma}_{EH} - \boldsymbol{\sigma}_m)\,\mathbf{A}_{EH}, \tag{10a}$$

$$\boldsymbol{\Gamma}_{CN} = f_{eff}\,(\boldsymbol{\sigma}_{CN} - \boldsymbol{\sigma}_m)\,\mathbf{A}_{CN}, \tag{10b}$$

with subscripts EH and CN referring to the electron hopping and conductive networking mechanisms, respectively. Nanotubes forming conductive networks can be modelled as fillers with infinite aspect ratio [20]. Therefore, quantities related to the electron hopping mechanism are defined with the actual filler aspect ratio ($\kappa = L_{cnt}/D_{cnt}$), while those related to the conductive networking mechanism are defined with infinite filler aspect ratio ($\kappa \to \infty$). Finally, the electric field concentration tensor, $\mathbf{A}$, is defined as [18]:

$$\mathbf{A} = \mathbf{A}^{dil}\left\{\left(1-f_{eff}\right)\mathbf{I} + f_{eff}\left\langle\mathbf{A}^{dil}\right\rangle\right\}^{-1}, \tag{11}$$

with $\mathbf{I}$ being the second-order identity tensor, $\mathbf{S}$ the Eshelby's tensor (well documented in [24]), and $\mathbf{A}^{dil}$ the dilute electric field concentration tensor:

$$\mathbf{A}^{dil} = \left\{\mathbf{I} + \mathbf{S}\,(\boldsymbol{\sigma}_m)^{-1}\,(\boldsymbol{\sigma}_c - \boldsymbol{\sigma}_m)\right\}^{-1}. \tag{12}$$

2.3. *Piezoresistivity properties of MWCNT/epoxy nanocomposites*

The strain self-sensing capability of MWCNT/epoxy composites can be simulated by means of strain-induced tampering of the electron hopping and conductive networking mechanisms. Specifically, three major strain effects are usually pointed out in the literature [25, 26], including (i) volume expansion and reorientation of MWCNTs, (ii) breakage of conductive paths, and (iii) variation of the inter-particle properties.

- *Volume expansion and reorientation*:

  Let us consider a deformable l_0-sided cubic cell loaded with a MWCNT as sketched in Fig. 2. When the cell is subjected to an arbitrary dilation strain $(\varepsilon_1, \varepsilon_2, \varepsilon_3)$, its volume changes from $V_0 = l_0^3$ to $V = l_0^3\overline{\varepsilon}_1\overline{\varepsilon}_2\overline{\varepsilon}_3$, with

$\bar{\varepsilon}_i = 1 + \varepsilon_i$. Owing to the considerably stiffer behaviour of MWCNTs, the deformation is primarily sustained by the matrix and, as a result, the apparent filler content varies as:

$$f^* = \frac{V_0 f}{V} = \frac{f}{\bar{\varepsilon}_1 \bar{\varepsilon}_2 \bar{\varepsilon}_3}. \tag{13}$$

Additionally, the embedded MWCNT also experiences reorientation as an effect of the applied dilation, which is defined by the change of the Euler angles from (γ,β) to (γ',β') (see Fig. 2). The closed-form expression of the strain-dependent ODF under general dilation strains, $\Omega(\gamma',\beta')$, was recently derived by the authors in [27] as:

$$\Omega(\gamma',\beta') = \frac{\bar{\varepsilon}_1^2 \bar{\varepsilon}_2^2 \bar{\varepsilon}_3^2}{\left[\bar{\varepsilon}_2^2 \bar{\varepsilon}_3^2 \cos^2\beta' + \bar{\varepsilon}_1^2 \left(\bar{\varepsilon}_2^2 \cos^2\gamma' + \bar{\varepsilon}_3^2 \sin^2\gamma'\right)\sin^2\beta'\right]^{3/2}}. \tag{14}$$

The deformable cell model can be also applied to study the effects of distortion. In this case, distortion does not originate volume expansion although it does induce filler reorientation. In the particular case of ε_{32}, the polar angle changes from β to β', while the azimuthal angle remains unchanged. The closed-form expression of the resulting ODF was also derived by the authors as [27]:

$$\Omega(\gamma,\beta') = \left(1 - 4\varepsilon_{32}\sin\gamma\sin\beta'\cos\beta' + 4\varepsilon_{32}^2\sin\gamma\sin\beta'\right)^{-3/2}. \tag{15}$$

- *Breakage of conductive paths*:

  The strain-induced filler reorientation reduces the randomness of the MWCNTs' dispersion and, as a consequence, the likelihood of forming conductive networks decreases, that is to say, the percolation threshold increases. Such a variation can be included in terms of the previously outlined strain-dependent ODFs as shown by the authors in reference [26] through the stochastic percolation model of Komori and Makishima [28].

- *Variation of the inter-particle properties*:

  Mechanical strains also have a direct effect on the electron hopping mechanism. In particular, assuming that deformations are mainly sustained by the matrix phase, mechanical strains primarily affect the inter-particle distance and the height of the potential barrier. At low strain levels ($< 10^{-4}$), some research studies in the literature consider that the inter-particle distance, d_a, and the height of the potential barrier, λ, vary linearly with strain as [29]:

$$\begin{aligned} d_a &= d_{a,0}(1 + C_1\varepsilon), \\ \lambda &= \lambda_0(1 + C_2\varepsilon), \end{aligned} \tag{16}$$

  where subscript 0 relates the corresponding quantities to the unstrained system, and C_1 and C_2 are proportionality constants. Given the difficulty involved in their determination, C_1 and C_2 are usually computed by fitting experimental data.

Finally, the modelling of the piezoresistivity of MWCNT-based composites can be readily conducted by combining the previously outlined micromechanics approach in Section 2.2 and the indicated strain-induced effects. For notational simplicity, the overall electrical resistivity tensor, $\boldsymbol{\rho}_{eff} = \boldsymbol{\sigma}_{eff}^{-1}$, is written in matrix notation as:

$$\boldsymbol{\rho}_{eff} = \begin{bmatrix} \rho_1 & \rho_6 & \rho_5 \\ \rho_6 & \rho_2 & \rho_4 \\ \rho_5 & \rho_4 & \rho_3 \end{bmatrix}. \tag{17}$$

In the absence of mechanical strains, MWCNTs are randomly oriented, and $\boldsymbol{\rho}_{eff}$ takes the form of a diagonal matrix with components $\rho_1 = \rho_2 = \rho_3 = \rho_0$ and $\rho_4 = \rho_5 = \rho_6 = 0$. Once the composite is subjected to a mechanical strain, the relative change in resistivity can be related to the mechanical strain tensor $\boldsymbol{\varepsilon}$ as [27]:

$$
\begin{bmatrix} \Delta\rho_1/\rho_0 \\ \Delta\rho_2/\rho_0 \\ \Delta\rho_3/\rho_0 \\ \Delta\rho_4/\rho_0 \\ \Delta\rho_5/\rho_0 \\ \Delta\rho_6/\rho_0 \end{bmatrix} = \begin{bmatrix} \lambda_{11} & \lambda_{12} & \lambda_{12} & 0 & 0 & 0 \\ \lambda_{12} & \lambda_{11} & \lambda_{12} & 0 & 0 & 0 \\ \lambda_{12} & \lambda_{12} & \lambda_{11} & 0 & 0 & 0 \\ 0 & 0 & 0 & \lambda_{44} & 0 & 0 \\ 0 & 0 & 0 & 0 & \lambda_{44} & 0 \\ 0 & 0 & 0 & 0 & 0 & \lambda_{44} \end{bmatrix} \begin{bmatrix} \varepsilon_1 \\ \varepsilon_2 \\ \varepsilon_3 \\ 2\varepsilon_{23} \\ 2\varepsilon_{13} \\ 2\varepsilon_{12} \end{bmatrix}, \tag{18}
$$

where the terms λ_{ij} denote the piezoresistivity coefficients. Specifically, λ_{11} represents the longitudinal piezoresistive effect, λ_{12} relates the transverse piezoresistive effect, and λ_{44} describes the effect on an out-of-plane electric field by the change of the in-plane current induced by in-plane shear stress. All the piezoresistivity coefficients λ_{ij} can be obtained by two virtual experiments using the previously outlined micromechanics approach, including a laterally constrained uni-axial dilation test and a distortion test (interested readers may refer to [27] for further theoretical details).

3. Basic formulae

3.1. Governing equations

3.2. Crack-face boundary conditions

3.3. Boundary element formulation

4. Resistivity changes detection scheme

5. Numerical results

5.1. Case study I: ....

5.2. Case study II: ....

6. Resume and conclusions

7. Acknowledgments

This work was supported by the Ministerio de Economía y Competitividad of Spain and the European Regional Development Fund under projects RTI2018-094945-B-C21 and DPI2017-89162-R. The financial support is gratefully acknowledged.

References

[1] Erik T Thostenson and Tsu-Wei Chou. Real-timein situsensing of damage evolution in advanced fiber composites using carbon nanotube networks. *Nanotechnology*, 19(21):215713, apr 2008.

[2] Xun Yu and Eil Kwon. A carbon nanotube/cement composite with piezoresistive properties. *Smart Materials and Structures*, 18(5):055010, mar 2009.

[3] Haibo Zhao, Yingying Zhang, Philip D Bradford, Qian Zhou, Quanxi Jia, Fuh-Gwo Yuan, and Yuntian Zhu. Carbon nanotube yarn strain sensors. *Nanotechnology*, 21(30):305502, jul 2010.

[4] Alamusi, Ning Hu, Hisao Fukunaga, Satoshi Atobe, Yaolu Liu, and Jinhua Li. Piezoresistive strain sensors made from carbon nanotubes based polymer nanocomposites. *Sensors*, 11(11):10691–10723, 2011.

[5] J. Sebastian, N. Schehl, M. Bouchard, M. Boehle, L. Li, A. Lagounov, and K. Lafdi. Health monitoring of structural composites with embedded carbon nanotube coated glass fiber sensors. *Carbon*, 66:191 – 200, 2014.

[6] Hongbo Dai, Erik T. Thostenson, and Thomas Schumacher. Processing and characterization of a novel distributed strain sensor using carbon nanotube-based nonwoven composites. *Sensors*, 15(7):17728–17747, 2015.

[7] Kai Ke, Vahab Solouki Bonab, Dian Yuan, and Ica Manas-Zloczower. Piezoresistive thermoplastic polyurethane nanocomposites with carbon nanostructures. *Carbon*, 139:52 – 58, 2018.

[8] Enrique García-Macías, Luis Rodríguez-Tembleque, and Andrés Sáez. Mwcnt/epoxy strip-like sensors for buckling detection in beam-like structures. *Thin-Walled Structures*, 133:27 – 41, 2018.

[9] Enrique García-Macías, Luis Rodríguez-Tembleque, Andrés Sáez, and Filippo Ubertini. Crack detection and localization in RC beams through smart MWCNT/epoxy strip-like strain sensors. *Smart Materials and Structures*, 27(11):115022, oct 2018.

[10] F. García-Sánchez, Andrés Sáez, and J. Domínguez. Anisotropic and piezoelectric materials fracture analysis by bem. *Computers & Structures*, 83(10):804 – 820, 2005. Boundary Element Methods.

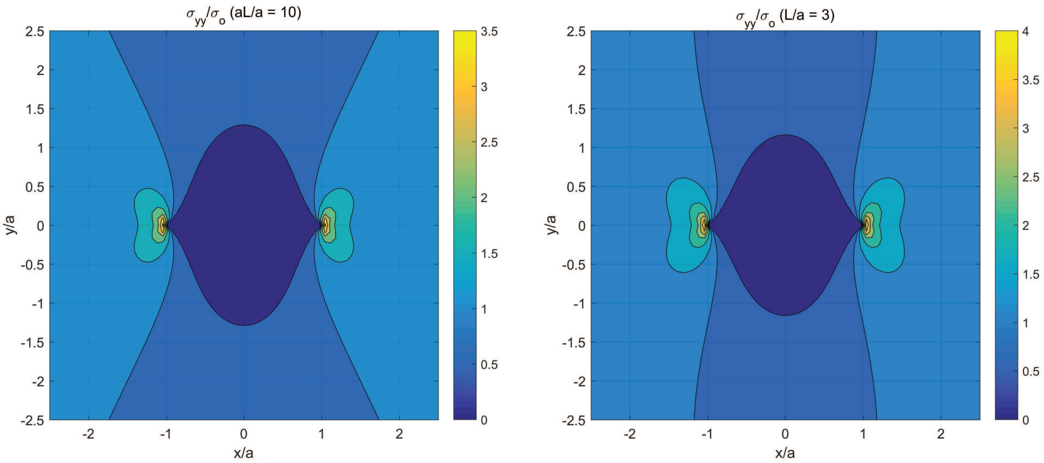

(a)

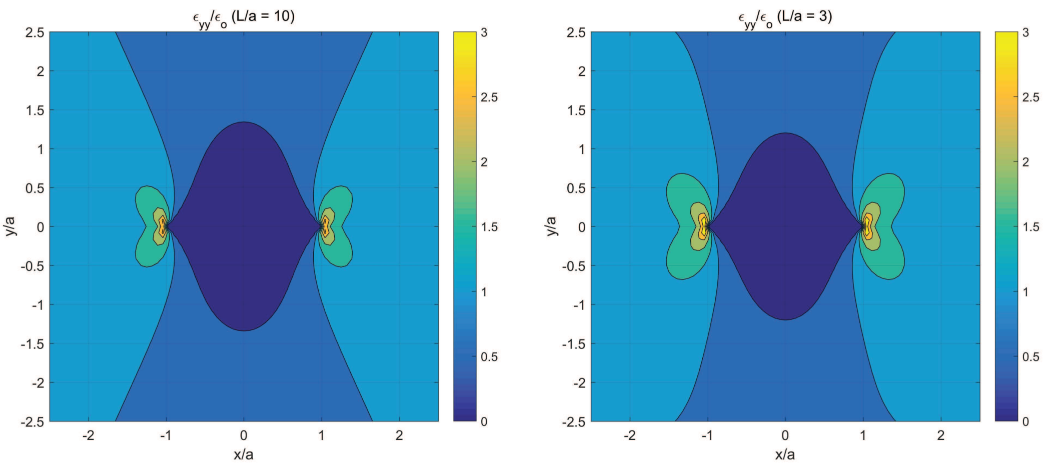

(b)

Figure 3: (a) σ_{22} stress distribution for $L/a = 10$ and $L/a = 3$. (b) ε_{22} strain distribution relative to the undamaged uniform strain ε_o, for $L/a = 10$ and $L/a = 3$.

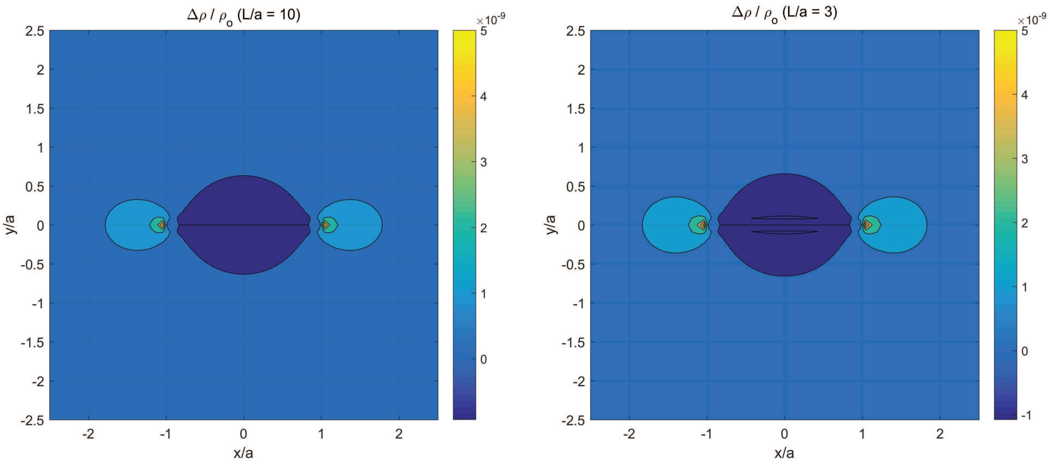

(a) (b)

Figure 4: Relative resistivity changes for the L/a ratios: (a) L/a = 10 and (b) L/a = 3.

[11] Enrique García-Macías, Rafael Castro-Triguero, Andrés Sáez, and Filippo Ubertini. 3d mixed micromechanics-fem modeling of piezoresistive carbon nanotube smart concrete. *Computer Methods in Applied Mechanics and Engineering*, 340:396 – 423, 2018.

[12] Wenxiang Xu, Fan Wu, Yang Jiao, and Mingjun Liu. A general micromechanical framework of effective moduli for the design of nonspherical nano-and micro-particle reinforced composites with interface properties. *Materials & Design*, 127:162–172, 2017.

[13] Enrique García-Macías, Rafael Castro-Triguero, and Filippo Ubertini. Two-step hierarchical micromechanics model of partially saturated porous composites doped with ellipsoidal particles with interface effects. *Composites Part B: Engineering*, 148:49–60, 2018.

[14] Muneo Hori and Sia Nemat-Nasser. Double-inclusion model and overall moduli of multi-phase composites. *Mechanics of Materials*, 14(3):189–206, 1993.

[15] Wenxiang Xu, Huaifa Ma, Shunying Ji, and Huisu Chen. Analytical effective elastic properties of particulate composites with soft interfaces around anisotropic particles. *Composites Science and Technology*, 129:10–18, 2016.

[16] Toshio Mura. *Micromechanics of defects in solids*, volume 3. Springer Science & Business Media, 1987.

[17] Fei Deng and Q. S. Zheng. An analytical model of effective electrical conductivity of carbon nanotube composites. *Applied Physics Letters*, 92(7):071902, 2008.

[18] Chuang Feng and Liying Jiang. Micromechanics modeling of the electrical conductivity of carbon nanotube (CNT)–polymer nanocomposites. *Composites Part A: Applied Science and Manufacturing*, 47:143–149, 2013.

[19] John G Simmons. Generalized formula for the electric tunnel effect between similar electrodes separated by a thin insulating film. *Journal of Applied Physics*, 34(6):1793–1803, 1963.

[20] Gary D Seidel and Dimitris C Lagoudas. A micromechanics model for the electrical conductivity of nanotube-polymer nanocomposites. *Journal of Composite Materials*, 43(9):917–941, 2009.

[21] KY Yan, QZ Xue, QB Zheng, and LZ Hao. The interface effect of the effective electrical conductivity of carbon nanotube composites. *Nanotechnology*, 18(25):255705, 2007.

[22] G. M. Odegard and T. S. Gates. Constitutive modeling of nanotube/polymer composites with various nanotube orientation. In *2002 SEM Annual Conference on Experimental and Applied Mechanincs*, 2002.

[23] Enrique García-Macías, Antonella D'Alessandro, Rafael Castro-Triguero, Domingo Pérez-Mira, and Filippo Ubertini. Micromechanics modeling of the electrical conductivity of carbon nanotube cement-matrix composites. *Composites Part B: Engineering*, 108:451–469, 2017.

[24] Minoru Taya. *Electronic composites: modeling, characterization, processing, and MEMS applications*. Cambridge University Press, 2005.

[25] C. Feng and L. Y. Jiang. Investigation of uniaxial stretching effects on the electrical conductivity of CNT-polymer nanocomposites. *Journal of Physics D: Applied Physics*, 47(40):405103, 2014.

[26] Enrique García-Macías, Antonella D'Alessandro, Rafael Castro-Triguero, Domingo Pérez-Mira, and Filippo Ubertini. Micromechanics modeling of the uniaxial strain-sensing property of carbon nanotube cement-matrix composites for SHM applications. *Composite Structures*, 163:195–215, March 2017.

[27] Enrique García-Macías, Rafael Castro-Triguero, Andrés Sáez, and Filippo Ubertini. 3D mixed micromechanics-FEM modeling of piezoresistive carbon nanotube smart concrete. *Computer Methods in Applied Mechanics and Engineering*, 340:396–423, 2018.

[28] Takashi Komori and Kunio Makishima. Numbers of fiber-to-fiber contacts in general fiber assemblies. *Textile Research Journal*, 47(1):13–17, 1977.

[29] AP Sobha and Sunil K Narayanankutty. Improved strain sensing property of functionalised multiwalled carbon nanotube/polyaniline composites in TPU matrix. *Sensors and Actuators A: Physical*, 233:98–107, 2015.

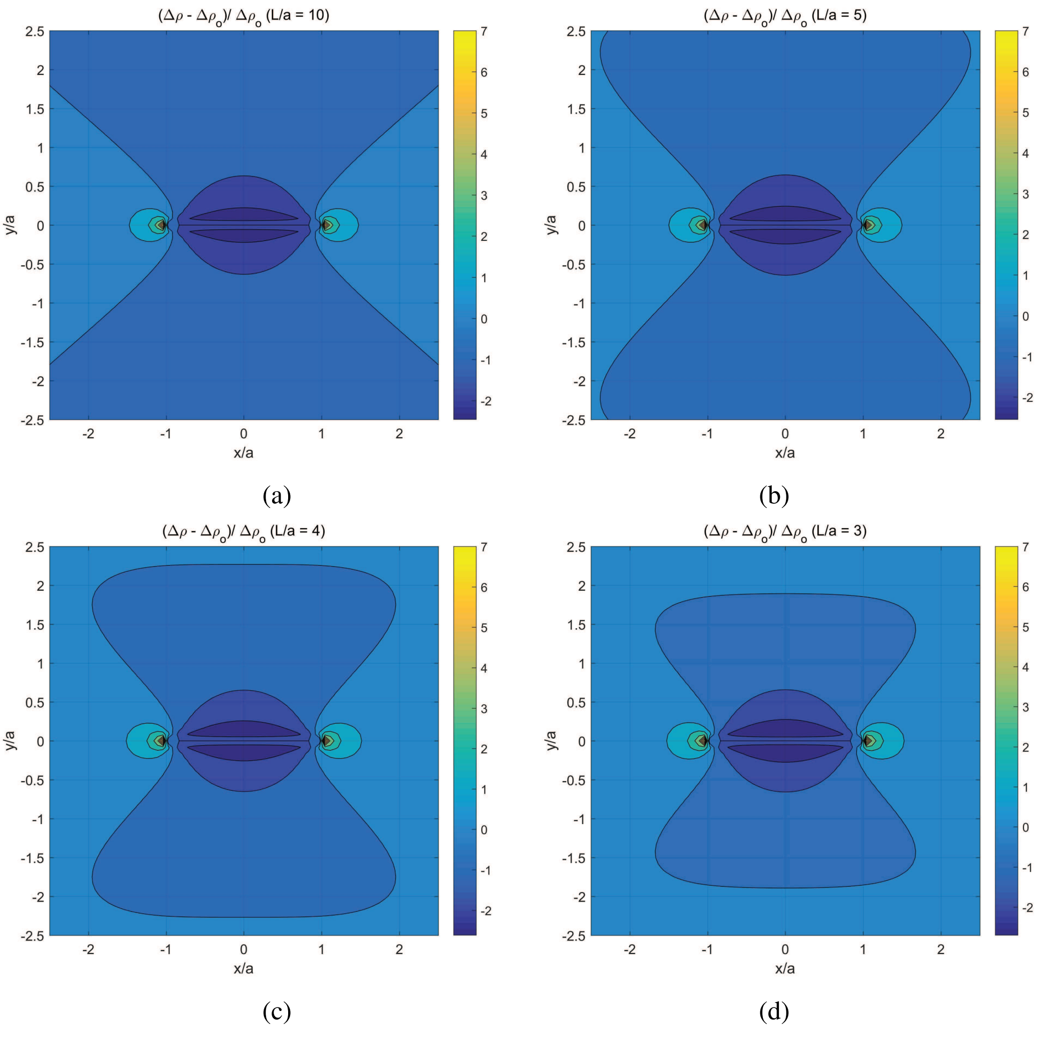

Figure 5: Resistivity changes due to the crack, relative to the undamaged plate, under several L/a ratios: (a) $L/a = 10$, (b) $L/a = 5$, (c) $L/a = 4$, (d) $L/a = 3$.

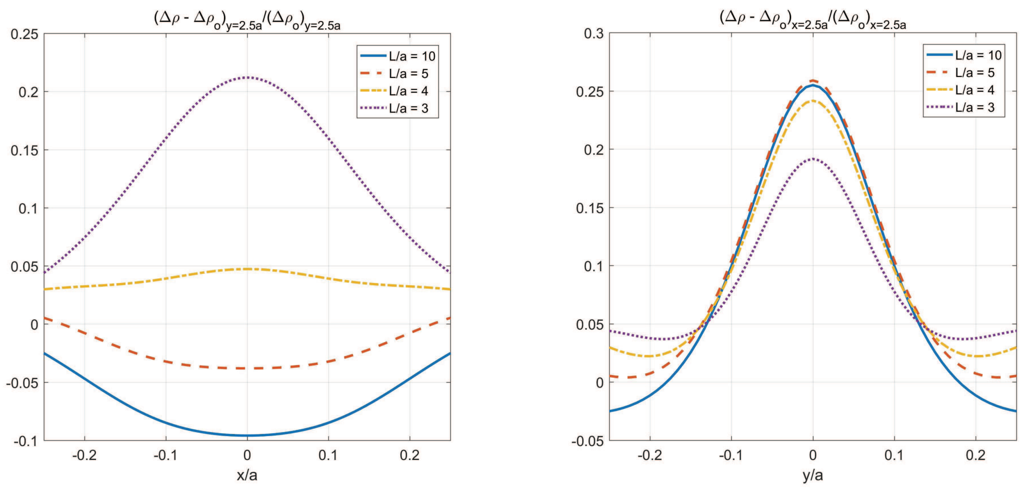

(a) (b)

Figure 6: Resistivity changes relative to the undamaged plate under several L/a ratios at: (a) $y = 2.5a$ and (b) $x = 2.5a$.